One-loop Renormalization of the Improved Energy–momentum Tensor in Lattice QCD

Mushtaq Loan[1,*] and Nasser Demir[2]

[1] *Department of Physics and Mathematics, Sichuan Uiversity Pittsburgh Institute (SCUPI), Chengdu, 61000, China*
[2] *Department of Physics. College of Science, Kuwait University, Safat, 1320, Kuwait*

(Dated: June 24, 2026)

We present a one-loop renormalization analysis of the improved gluonic energy–momentum tensor in pure SU(3) lattice gauge theory, employing a tadpole-improved tree-level Symanzik gauge action and a three-loop-improved clover discretization of the field-strength tensor. The calculation is conducted in Landau gauge by matching the amputated two-gluon matrix element of the lattice energy–momentum tensor to the continuum $\overline{\text{MS}}$ scheme. The one-loop correction is separated into sail, operator-tadpole, and external-leg contributions, each expressed in terms of a minimal set of scalar Brillouin-zone integrals. This approach yields explicit expressions for the finite lattice coefficient $\mathfrak{B}_{\text{lat}}(u_0)$ and the multiplicative renormalization factor $Z_T(u_0)$ associated with the traceless spin-2 component of the energy–momentum tensor. A key result is the clear distinction between the spin-2 sector, governed by Z_T, and the scalar trace sector, which encodes the Yang–Mills trace anomaly. We demonstrate that the improved lattice construction maintains the correct continuum anomaly structure, with the trace determined by the scalar operator $F_{\rho\sigma}F_{\rho\sigma}$ and the Yang–Mills β function, rather than by the spin-2 renormalization factor. The resulting renormalized energy–momentum tensor alters the normalization and short-distance behaviour of Euclidean energy-density correlators through both traceless and scalar-channel contributions. Comparison with existing lattice thermodynamic data indicates that the improved operator accurately reproduces the expected temperature dependence of the trace anomaly and provides a systematically improvable framework for studying the equation of state, gluon condensate, and transport coefficients in lattice QCD.

arXiv:2606.24222v1 [hep-lat] 23 Jun 2026

I. INTRODUCTION

The energy–momentum tensor (EMT) is a central operator in quantum field theory. As the conserved current associated with spacetime translational invariance [1, 2], its matrix elements encode the hadron's momentum and spin fractions [3–5], its expectation value in thermal states defines the equation of state, and all thermodynamic metrics of strongly-coupled matter [6], and encodes physically important quantities such as the energy density, momentum flow, thermodynamic observables, and gravitational form factors [7, 8]. In Yang-Mills theory and QCD, a correctly normalized EMT is also required for the nonperturbative study of the equation of state, transport coefficients, hadron and glueball matrix elements, and the trace anomaly.

On the lattice, however, the construction of the energy-momentum tensor (EMT) is nontrivial because continuous translational symmetry is explicitly broken to a discrete subgroup. The naïve discretization of the EMT operator leads to severe ultraviolet divergences—extreme fluctuations at very short distances—that require multiplicative and additive renormalization [9]. Unlike simpler fermion bilinears, the EMT mixes with other operators of equal or lower dimension under renormalization [10, 11], and its renormalization constants depend on the lattice action and the specific discretization of the gauge and fermion fields. Moreover, the conservation of the EMT, which is exact in the continuum, is broken by lattice artifacts - that is, artifacts arising specifically from the discretization - making a direct extraction of physical matrix elements from lattice correlators a delicate task.

Two distinct frameworks have been developed to address these challenges. The first framework utilizes shifted boundary conditions to introduce a nonperturbative renormalisation scheme, thereby eliminating the need to explicitly construct composite operators on the lattice. Imposing twisted boundary conditions in the Euclidean time direction relates the partition function of the EM tensor to a derivative with respect to the shift parameter. Such a relationship facilitates the extraction of renormalized EMT matrix elements via a Ward identity [12, 13]. This approach has been successfully applied to the renormalisation of the EM tensor in pure Yang-Mills theory [13] and later extended to full QCD [14], to accurately reproduce the trace anomaly. The second approach, the so-called gradient flow, uses a continuous smoothing transformation on gauge and fermion fields along a positive 'flow time' t. This technique reduces ultraviolet quantum fluctuations while preserving the essential long-distance physics of strong interactions. Suzuki first showed that a finite, renormalised energy-momentum tensor (EMT)—which measures the density and flow of energy and momentum in a field—could be built from flowed fields in pure gauge theory [15]. This idea was later extended to include quarks [16], offering a practical, gauge-invariant EMT definition on the lattice (a discrete spacetime grid used in numerical simulations). This method has now become standard for lattice QCD thermodynamics, supporting high-precision calculations of the trace anomaly and the equation of state [6]. These advances set a benchmark for perturbative calculations: one-loop lattice per-

* Corresponding author

turbation theory renormalisation factors—correction factors accounting for quantum effects at one order—should match the correct weak-coupling behaviour and can be directly compared with nonperturbative lattice data [17].

Perturbative lattice perturbation theory complements these non-perturbative methods by providing crucial input on operator mixing coefficients and renormalization constants. Specifically, one-loop computations of the renormalization of the EMT have been carried out for a variety of lattice actions, [10, 11, 18, 19], serving as a necessary component in the development of improved actions as well as a consistency check. More recently, high-precision non-perturbative matching between the lattice EMT and continuum schemes like $\overline{\text{MS}}$ [20] has been made possible by the development of gauge-invariant renormalization schemes building on these foundations and allowing direct comparison with phenomenological extractions.

The present work is situated at the interface between improved lattice perturbation theory and nonperturbative EMT renormalization. Our goal is to compute the one-loop renormalization of a tadpole-improved gluonic EMT built from a three-loop improved clover field-strength tensor, together with the tree-level Symanzik gauge action containing plaquette and rectangle terms. In this framework, the one-loop matching factor is obtained by evaluating the two-gluon matrix element of the operator in lattice perturbation theory and converting it to a continuum renormalization scheme. The calculation naturally separates into sail, tadpole, and external-leg contributions, each of which contributes to the finite lattice coefficient entering the renormalization factor. Normalization ensures that the clover EMT has tree-level coefficients of order unity, making perturbative matching (e.g., to $\bar{M}S$) more stable and convergent. To elaborate, a central issue in this analysis is the distinction between the traceless spin-2 channel and the scalar trace channel. In particular, the multiplicative renormalization constant Z_T extracted from the spin-2 projector fixes the normalisation of the traceless part of the EMT, while the trace anomaly is encoded in the scalar operator proportional to $F^a_{\rho\sigma}F^a_{\rho\sigma}$. Consequently, a complete renormalisation program must track both sectors: the perturbative matching of the spin-2 operator and the scalar-channel normalisation required to reproduce the EMT in the continuum limit.

The paper is organized as follows. We first define the tadpole-improved three-loop clover EMT to derive the relevant propagators and operator vertices in Landau gauge, including the two-, three-, and four-gluon EMT kernels. Next, we evaluate the one-loop sail, tadpole, and external-leg diagrams and reduce the projected amplitudes to a minimal basis of Brillouin-zone integrals. This yields the lattice finite coefficient $\mathfrak{B}_{\rm lat}(u_0)$ and, through matching to the continuum scheme, the renormalization constant Z_T. Finally, we discuss the trace anomaly, the scalar channel, and the comparison between the perturbative prediction and results obtained using shifted boundary conditions and gradient-flow methodologies.

II. THEORETICAL FRAMEWORK

A. Tadpole-improved Energy-Momentum Tensor on Lattice

The action is discretized through the tadpole-improved Symanzik gauge action [21]

$$S_g^{Imp} = \frac{\beta}{N_C}\left[\frac{c_0}{u_0^4}\sum_{plaq}\frac{1}{3}\text{Re Tr}(1-U_{plaq}) + \frac{c_1}{u_0^6}\sum_{rect.}\frac{1}{3}\text{Re Tr}(1-U_{rect})\right] \quad (1)$$

where the trace is over the colour indices and $\beta = 2N_C/g_0^2$ with g_0 being the bare coupling constant. For the Symanzik action, the coefficients are $c_0 = 5/3$ and $c_1 = -1/12$.

The plaquette is defined as a function of the gauge links, and it given by

$$U_{\mu\nu}(x) = U_\mu(x)U_\nu(x+a\hat{\mu})U^\dagger_\mu(x+a\hat{\nu})U^\dagger_\mu(x)$$

where $\mu, \mu = 0, \cdots 3$, $\hat{\mu}$ is the unit vector along the direction μ, and x is the space-time coordinate.

The energy-momentum tensor of the gauge field theory has the form:

$$T_{\mu\nu}(x) = \frac{1}{g_0^2}\left[F^a_{\mu\alpha}F^a_{\mu\alpha} - \frac{1}{4}\delta_{\mu\nu}F^a_{\alpha\beta}F^a_{\alpha\beta}\right], \quad (2)$$

where the gluon field strength tensor is defined as

$$F^a_{\mu\nu}(x) = -\frac{i}{4a^2}\left[\Big(Q_{\mu\nu}(x) - Q^\dagger_{\mu\nu}(x)\Big)T^a\right], \quad (3)$$

and

$$Q_{\mu\nu} = \frac{1}{4}\Big(U_{\mu\nu}(x)+U_{-\nu\mu}(x)+U_{\nu-\mu}(x)+U_{-\mu-\nu}(x)\Big) \quad (4)$$

is the sum of the four plaquette terms. The gluon field strength tensor has $O(a^2)$ discretisation errors. To improve the discretisation of the gluon field strength tensor, we incorporate additional higher "clover" loops (Fig. 1) in $F_{\mu\nu}$. In general, we define the following improved field strength tensor

$$F^{imp}_{\mu\nu}(x) = k_1F^{1\times1}_{\mu\nu} + k_2F^{2\times2}_{\mu\nu} + \frac{k_3}{2}\Big(F^{2\times1}_{\mu\nu} + F^{1\times2}_{\mu\nu}\Big) \frac{k_4}{2}\Big(F^{3\times1}_{\mu\nu} + F^{1\times3}_{\mu\nu}\Big) + k_5F^{3\times3}_{\mu\nu}, \quad (5)$$

where

$$F^{m\times n}_{\mu\nu}(x) = -\frac{i}{4a^2}\left[\Big(Q^{m\times n}_{\mu\nu}(x) - Q^{\dagger m\times n}_{\mu\nu}(x)\Big)T^a\right] \quad (6)$$

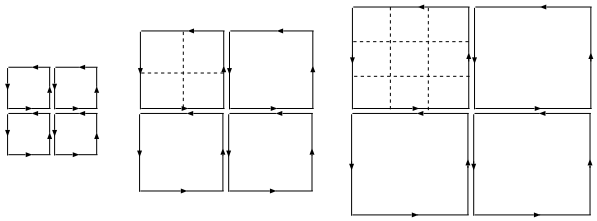

FIG. 1. The 1×1, 2×2, and 3×3 loops are used to construct the clover term for the improved energy-momentum tensor.

k_i are the constant coefficients and $Q_{\mu\nu}^{m\times n}(x)$ corresponds to the sum of the four $m\times n$ loops in the clover formation.

For computational efficiency, we consider a 3-loop improved field strength tensor ($k_4 = k_5 = 0$) with mean field improved coefficients,

$$F_{\mu\nu}^{3L}(x) = \frac{3}{2u_0^4}F_{\mu\nu}^{1\times1}(x) - \frac{3}{20u_0^8}F_{\mu\nu}^{2\times2}(x) + \frac{1}{90u_0^{12}}F_{\mu\nu}^{3\times3}(x) \tag{7}$$

The improved energy-momentum tensor is then represented by

$$T_{\mu\nu}^{Imp}(x) = \frac{1}{g_0^2}\left[F_{\mu\alpha}^{3L}F_{\mu\alpha}^{3L} - \frac{1}{4}\delta_{\mu\nu}F_{\alpha\beta}^{3L}F_{\alpha\beta}^{3L}\right]. \tag{8}$$

III. ONE-LOOP RENORMALIZATION OF $T_{\mu\nu}^{Imp}(x)$

The improved EMT on the lattice, $T_{\mu\nu}^{Imp.}$, is a composite operator. When inserted into correlation functions, it will have UV divergences from point-splitting regularization, operator mixing with lower-dimensional operators, and lattice artifacts from broken continuum symmetries. The renormalized operator $T_{\mu\nu}^{R,Imp.}$ is related to its bare counterpart by

$$T_{\mu\nu}^{R}(x) = Z_T(g_0^2)\Big(T_{\mu\nu}^{Imp}(x) - \langle T_{\mu\nu}^{Imp}(x)\rangle\Big). \tag{9}$$

The subtraction of the vacuum expectation value, $\langle T_{\mu\nu}^{Imp}(x)\rangle$ is essential as it non-perturbatively removes the power divergent mixing $\approx \delta_{\mu\nu}/a^2$.

A. Propagator and n-gluon EMT Vertices

The tree-level gluon propagator is obtained from the quadratic terms in the action. For each loop (plaquette or rectangle) the second order term is proportional to the lattice discretization of $(\partial_\mu A_\nu - \partial_\nu A_\mu)^2$ plus higher-derivative discretization corrections. The contribution from the total quadratic action, after expanding and Fourier transforming in momentum space has the form

$$S^{(2)} = \frac{1}{2}\sum_k A_\mu^a(-k)G_{\mu\nu}^{ab}(k)A_\nu^b,$$

where

$$\hat{k}_\mu = \frac{2}{a}\sin\left(\frac{ak_\mu}{2}\right), \qquad \hat{k}^2 = \sum_\mu \hat{k}_\mu^2.$$

The quadratic kernal has the usual transverse and logitudinal decomposition

$$G_\mu(k) = A(k)P_\mu^T(k) + B(k)P_{\mu\nu}^L(k),$$

where the functions $A(k)$ and $B(k)$ are simply the transverse and longitudinal eigenvalues of the quadratic (inverse–propagator) kernel $G_{\mu\nu}(k)$:

$$P_{\mu\nu}^T(k) = \delta_{\mu\nu} - \frac{\hat{k}_\mu\hat{k}_\nu}{\hat{k}^2}, \qquad P_{\mu\nu}^L(k) = \frac{\hat{k}_\mu\hat{k}_\nu}{\hat{k}^2}.$$

The functions $A(k)$ and $B(k)$ are obtained by projecting $G_{\mu\nu}$ onto the transverse/longitudinal subspaces:

$$\begin{aligned} A(k) &= \frac{1}{d-1}\mathrm{Tr}\left[G(k)P^T(k)\right] = \frac{1}{d-1}P_{\mu\nu}^T(k)G_{\mu\nu}(k), \\ B(k) &= \mathrm{Tr}\left[G(k)P^L(k)\right] = P_{\mu\nu}^L(k)G_{\mu\nu}(k) = \frac{\hat{k}_\mu G_{\mu\nu}(k)\hat{k}_\nu}{\hat{k}^2}, \end{aligned}$$

for $d = 4$ Eucilidean lattice.

On the lattice, gauge invariance implies that the quadratic gauge kernel $G_{\mu\nu}(k)$ has a null longitudinal mode,

$$\tilde{k}_\mu G_{\mu\nu}(k) = 0,$$

and is therefore not directly invertible. To define the gluon propagator, one adds the lattice gauge-fixing term

$$S_{\mathrm{gf}} = \frac{1}{2\xi}\sum_x \left(\nabla_\mu^- A_\mu^a(x)\right)^2,$$

which contributes in momentum space

$$G_{\mu\nu}^{(\mathrm{gf})}(k) = \frac{1}{\xi}\,\hat{k}_\mu\hat{k}_\nu.$$

The full quadratic kernel is then

$$G_{\mu\nu}^{(\mathrm{tot})}(k) = G_{\mu\nu}^{(0)}(k) + \frac{1}{\xi}\hat{k}_\mu\hat{k}_\nu,$$

with $G_{\mu\nu}^{(0)}(k)$ the gauge-invariant part coming from the Symanzik action. For an exactly gauge-invariant quadratic kernel, the longitudinal eigenvalue vanishes, while the transverse eigenvalue takes the form

$$A(k) = \hat{k}^2 K_T(k;u_0),$$

where $K_T(k;u_0)$ is the improvement factor induced by the plaquette and rectangle terms.

To enforce transversality of the propagator and remove the longitudinal modes, we choose the Landau gauge

($\xi \to 0$). The tree-level gluon propagator in Landau gauge is therefore the inverse of the transverse kernel:

$$D^{ab}_{\mu\nu}(k;u_0)|_{\rm Landau} = \delta^{ab}\left(\delta_{\mu\nu} - \frac{\hat{k}_\mu \hat{k}_\nu}{\hat{k}^2}\right)\frac{1}{\hat{k}^2 K_T(k;u_0)}, \tag{10}$$

where the continuum-like transverse operator ($\hat{k}^2\delta_{\mu\nu} - \hat{k}_\mu\hat{k}_\nu$) receives the leading scalar transverse eigenvalue factor

$$K_T(k;u_0) = \left[\tilde{c}_0 + \tilde{c}_1 a^2\hat{k}^2 + O(a^4\hat{k}^2\right], \tag{11}$$

with the effective coefficients in the transverse kernel given by:

$$\tilde{c}_0 = \left(\frac{c_0}{u_0^4} + \frac{8c_1}{u_0^6}\right), \qquad \tilde{c}_1 = -\frac{c_1}{u_0^6}.$$

To calculate the EMT 2-,3-, and 4-gluon vertices, we expand improved field strength, $F^{n\times n}_{\mu\nu}$, for each clover loop size $n = 1, 2, 3$

$$F^{n\times n}_{\mu\nu} = F^{(1),n\times n}_{\mu\nu} + g_0 F^{(2),n\times n}_{\mu\nu} + g_0^2 F^{(3),n\times n}_{\mu\nu} + O(g_0^3).$$

Therefore,

$$F^{3L}_{\mu\nu} = F^{(1),3L}_{\mu\nu} + g_0 F^{(2),3L}_{\mu\nu} + g_0^2 F^{(3),3L}_{\mu\nu} + O(g_0^3),$$

with

$$F^{(r),3L}_{\mu\nu} = \frac{3}{2u_0^4}F^{(1),1\times1}_{\mu\nu} - \frac{3}{20u_0^8}F^{(2),2\times2}_{\mu\nu} + \frac{1}{90u_0^{12}}F^{(3),3\times3}_{\mu\nu}.$$

The EMT operator then expands as

$$T^{Imp}_{\mu\nu} = T^{(2)}_{\mu\nu} + g_0 T^{(3)}_{\mu\nu} + g_0^2 T^{(4)}_{\mu\nu} + O(g_0^3), \tag{12}$$

where

$$\begin{aligned}
T^{(2)}_{\mu\nu} &= \frac{1}{g_0^2}\left[F^{(1),3L}_{\mu\alpha}F^{(1),3L}_{\nu\alpha} - \frac{1}{4}\delta_{\mu\nu}F^{(1),3L}_{\alpha\beta}F^{(1),3L}_{\alpha\beta}\right],\\
T^{(3)}_{\mu\nu} &= \frac{2}{g_0}\left[F^{(1),3L}_{\mu\alpha}F^{(2),3L}_{\nu\alpha} - \frac{1}{4}\delta_{\mu\nu}F^{(1),3L}_{\alpha\beta}F^{(2),3L}_{\alpha\beta}\right],\\
T^{(4)}_{\mu\nu} &= F^{(2),3L}_{\mu\alpha}F^{(1),3L}_{\nu\alpha} + 2F^{(1),3L}_{\mu\alpha}F^{(3),3L}_{\nu\alpha}\\
&\quad -\frac{1}{4}\delta_{\mu\nu}\left(F^{(2),3L}_{\alpha\beta}F^{(2),3L}_{\alpha\beta} + F^{(1),3L}_{\alpha\beta}F^{(3),3L}_{\alpha\beta}\right),
\end{aligned} \tag{13}$$

generate, respectively, the 2-gluon, 3-gluon, and 4-gluon EMT vertices. In the momentum space, with the standard lattice momenta

$$\hat{p}_\mu = \frac{2}{a}\sin(ap_\mu/2),\ \ \tilde{p}_\mu = \sin(ap_\mu),\ \ c_\mu(p) = \cos(ap_\mu/2),$$

the linearised clover field strength for $n \times n$ loop can be written as

$$F^{(1),n,a}_{\mu\nu} = iR_n(p_\mu)R_n(p_\nu)(\hat{p}_\mu A_\nu - \hat{p}_\nu A_\mu),$$

where the path sum factor $R_n(p_\mu)$ is

$$R_n(p_\mu) = \frac{\sin(nap_\mu/2)}{\sin(ap_\mu/2)},$$

with p_μ as the external four-momentum carried by the EMT insertion matrix element. The plaquette-size kernal is defined by

$$\Omega^{\mu\nu}_n(p) = R_n(p_\mu)R_n(p_\nu)$$

and the 3-loop ($3L$) improved kernal is then given by

$$F^{(1),3L}_{\mu\nu}(p) = i\Omega^{\mu\nu}_{3L}(p;u_0)(\hat{p}_\mu A_\nu - \hat{p}_\nu A_\mu),$$

with

$$\begin{aligned}
\Omega^{\mu\nu}_{3L}(p;u_0) &= \sum_{n=1}^{3} c_n^{(F)}\Omega^{\mu\nu}_n(p)\\
&= \frac{3}{2u_0^4}\Omega^{\mu\nu}_1 - \frac{3}{20u_0^8}\Omega^{\mu\nu}_2 + \frac{1}{90u_0^{12}}\Omega^{\mu\nu}_3.
\end{aligned}$$

Writing $T^{(2)} = \frac{1}{2}A\Lambda^{(2)}_T A$, the amputated 2-gluon operator vertex is then given by

$$\Lambda^{ab,(2)}_{\mu\nu;\rho\sigma}(p;u_0) = \delta^{ab}\frac{1}{g_0^2}\Omega^{\rho\alpha}_{3L}(p;u_0)\Omega^{\sigma\beta}_{3L}(p;u_0)Q^{\alpha\beta}_{\mu\nu;\rho\sigma}(p), \tag{14}$$

where Q is the standard gluonic EMT structure with lattice momenta p_μ, p_ν and Lorentz indices ρ, σ

$$\begin{aligned}
Q^{\alpha\beta}_{\mu\nu;\rho\sigma}(p) &= (\delta_{\mu\rho}\hat{p}_\alpha - \delta_{\mu\alpha}\hat{p}_\rho)(\delta_{\nu\rho}\hat{p}_\alpha - \delta_{\nu\alpha}\hat{p}_\rho) + (\rho \leftrightarrow \sigma)\\
&\quad -\frac{1}{4}\delta_{\mu\nu}\left[(\delta_{\gamma\rho}\hat{p}_\alpha - \delta_{\gamma\alpha}\hat{p}_\rho)(\delta_{\gamma\sigma}\hat{p}_\beta - \delta_{\gamma\beta}\hat{p}_\sigma)\right.\\
&\quad \left.+(\rho \leftrightarrow \sigma)\right].
\end{aligned} \tag{15}$$

To obtain the EMT 3-gluon vertex, we need to evaluate the quadratic part of the clover field strength, $F^{(2),n}$ in the second equation of (13). For any Wilson loop, the quadratic term in the anti-Hermitian part can be written in momentum space as

$$F^{(2),a,n}_{\mu\nu} = \frac{1}{2}f^{abc}\int_{BZ}\frac{d^4q}{(2\pi)^4}\mathcal{S}^a_{\mu\nu;\rho\sigma}(p,q)A^b_\rho(q)A^c_\sigma(p-q),$$

where, for the average $n \times n$ clover loop, the kernal $\mathcal{S}$ is obtained by summing over pair of link insertions on the loop and, after antisymmetrizing, is given by

$$\begin{aligned}
\mathcal{S}^{(n)}_{\mu\nu;\rho\sigma}(p,q) &= \left[\delta_{\rho\mu}\delta_{\sigma\nu}C^{(n)}_{\mu\nu}(q,p-q)\right.\\
&\quad \left.-\delta_{\rho\nu}\delta_{\sigma\mu}C^{(n)}_{\mu\nu}(q,p-q)\right] + \mathcal{T}^{(n)}_{\mu\nu;\rho\sigma}.
\end{aligned} \tag{16}$$

The first two terms in Eq. 16) are the continuum-like commutor core, and $\mathcal{T}$ contains the lattice transport correlations. The core factor C_μ and the transport term $\mathcal{T}^{(n)}$ are, respectively, given by

$$\begin{aligned}
C^{(n)}_{\mu\nu}(q,r) &= R_n(q_\mu)R_n(r_\nu)c_\mu(q)c_\nu(q)\Omega^{\mu\nu}_n(q+r),\\
\mathcal{T}^{(n)}_{\mu\nu;\rho\sigma} &= \delta_{\rho\mu}\delta_{\sigma\mu}\mathcal{X}^{(n)}_{\mu\nu}(p,q) - \delta_{\rho\nu}\delta_{\sigma\nu}\mathcal{X}^{(n)}_{\nu\mu}(p,q)\\
&\quad +\delta_{\rho\mu}\delta_{\sigma\nu}\mathcal{Y}^{(n)}_{\mu\nu}(p,q) - \delta_{\rho\nu}\delta_{\sigma\mu}\mathcal{Y}^{(n)}_{\nu\mu}(p,q),
\end{aligned}$$

where

$$\mathcal{X}^{(n)}_{\mu\nu}(p,q) = \frac{a}{2}\hat{q}_\nu R_n(q_\mu)R_n((p-q)_\mu)R_n(p_\nu),$$
$$\mathcal{Y}^{(n)}_{\mu\nu}(p,q) = \frac{a}{2}\hat{q}_\mu R_n(q_\mu)R_n((p-q)_\nu)R_n(p_\nu).$$

Thus

$$F^{(2),a,3L}_{\mu\nu} = \frac{1}{2}f^{abc}\int_{BZ}\frac{d^4q}{(2\pi)^4}\mathcal{S}^{3L}_{\mu\nu;\rho\sigma}(p,q;u_0)A^b_\rho(q)A^c_\sigma(p-q),$$

with

$$\mathcal{S}^{(3L)}_{\mu\nu;\rho\sigma}(p,q;u_0) = \sum_{n=1}^{3} c_n^{(F)}\mathcal{S}^{(n)}_{\mu\nu;\rho\sigma}(p,q),$$

and

$$c_1^{(F)} = \frac{3}{2u_0^4},\ c_2^{(F)} = -\frac{3}{20u_0^8},\ c_3^{(F)} = \frac{1}{90u_0^{12}}.$$

Then the 3-gluon vertex is given by

$$\Lambda^{abc,(3)}_{\mu\nu;\rho\sigma\lambda}(p,q,r;u_0) = \frac{2}{g_0}f^{abc}\Big[\mathcal{G}_{\mu\nu;\rho\sigma\lambda}(p,q,r;u_0) - \frac{1}{4}\delta_{\mu\nu}\mathcal{G}_{\alpha\alpha;\rho\sigma\lambda}(p,q,r;u_0)\Big], \tag{17}$$

where

$$\begin{aligned}\mathcal{G}_{\mu\nu;\rho\sigma\lambda}(p,q,r;u_0) &= \Omega^{\mu\alpha}_{3L}(p;u_0)\big(\hat{p}_\mu\delta_{\alpha\rho} - \hat{p}_\alpha\delta_{\mu\rho}\big)\\ &\times\mathcal{S}^{(3L)}_{\nu\alpha;\sigma\lambda}(-p,q;u_0)\\ &+\Omega^{\nu\alpha}_{3L}(p;u_0)\big(\hat{p}_\nu\delta_{\alpha\rho} - \hat{p}_\alpha\delta_{\nu\rho}\big)\\ &\times\mathcal{S}^{(3L)}_{\mu\alpha;\sigma\lambda}(-p,q;u_0),\end{aligned} \tag{18}$$

with momentum conservation $p+q+r=0$.

The most involved ingredient is the four-gluon EMT vertex. The 4-gluon vertex

$$\begin{aligned}\Lambda^{abcd,(4)}_{\mu\nu;\rho\sigma\lambda\tau}(p_i;u_0) &= \Lambda^{abcd,(4)}_{\mu\nu;\rho\sigma\lambda\tau}|_{(2)(2)}(p_i;u_0)\\ &+\Lambda^{abcd,(4)}_{\mu\nu;\rho\sigma\lambda\tau}|_{(1)(3)}(p_i;u_0)\end{aligned}$$

receives contributions from $F^{(2)}F^{(2)}$ and $F^{(1)}F^{(3)}$ parts. The $F^{(2)}F^{(2)}$ contribution can be written as

$$\Gamma^{abcd,(4)}_{\mu\nu;\rho\sigma\lambda\tau}\Big|_{(2)(2)} = \sum_{\chi=s,t,u}\mathcal{C}^{abcd}_\chi\Big[\mathcal{H}^{(\chi)}_{\mu\nu;\rho\sigma\lambda\tau}(p_i;u_0) - \frac{1}{4}\delta_{\mu\nu}\mathcal{H}^{(\chi)}_{\alpha\alpha;\rho\sigma\lambda\tau}(p_i;u_0)\Big],$$

with the color tensors

$$\mathcal{C}^{abcd}_s = f^{abe}f^{cde},\ \mathcal{C}^{abcd}_t = f^{ace}f^{bde},\ \mathcal{C}^{abcd}_u = f^{ade}f^{bce}.$$

Each $\mathcal{H}^{(\chi)}$ is bilinear in $\mathcal{S}^{(3L)}$, and therefore inherits the decomposition

$$\mathcal{H} = \mathcal{H}_{cc} + \mathcal{H}_{cT} + \mathcal{H}_{Tc} + \mathcal{H}_{TT}, \tag{19}$$

with $\mathcal{S} = \mathcal{S}_c + \mathcal{T}$. Here $\mathcal{H}_{cc}$ is the core-core contribution, in which both quadratic field-strength factors are represented by their continuum-like local kernels. This term controls the leading continuum tensor structure of the operator. The mixed terms $\mathcal{H}_{cT}$ and $\mathcal{H}_{Tc}$ arise when one field-strength factor contributes through its core part and the other through its transport part, and therefore describe the leading interference between local continuum physics and the extended Wilson-loop geometry of the lattice clover operator. The transport-transport contribution $\mathcal{H}_{TT}$ is built solely from the transport kernels and represents the purely lattice-geometric, nonlocal correction. Thus, the decomposition provides a natural separation between continuum-like physics, leading lattice corrections, and fully geometric lattice artifacts.
For s channel

$$\begin{aligned}\mathcal{H}^s_{cc,\mu\nu;\rho\sigma\lambda\tau} &= \frac{1}{4}\mathcal{S}^{(3L)}_{core,\mu\alpha;\rho\sigma}(p_1+p_2,p_1)\\ &\times\mathcal{S}^{(3L)}_{core,\nu\alpha;\lambda\tau}(p_3+p_4,p_3+(\rho\sigma\leftrightarrow\lambda\tau),\\ \mathcal{H}^s_{cT,\mu\nu;\rho\sigma\lambda\tau} &= \frac{1}{4}\mathcal{S}^{(3L)}_{core,\mu\alpha;\rho\sigma}(p_1+p_2,p_1)\\ &\times\mathcal{T}^{(3L)}_{core,\nu\alpha;\lambda\tau}(p_3+p_4,p_3)+(\rho\sigma\leftrightarrow\lambda\tau),\\ \mathcal{H}^s_{Tc,\mu\nu;\rho\sigma\lambda\tau} &= \frac{1}{4}\mathcal{T}^{(3L)}_{core,\mu\alpha;\rho\sigma}(p_1+p_2,p_1)\\ &\times\mathcal{S}^{(3L)}_{core,\nu\alpha;\lambda\tau}(p_3+p_4,p_3)+(\rho\sigma\leftrightarrow\lambda\tau),\\ \mathcal{H}^s_{TT,\mu\nu;\rho\sigma\lambda\tau} &= \frac{1}{4}\mathcal{T}^{(3L)}_{core,\mu\alpha;\rho\sigma}(p_1+p_2,p_1)\\ &\times\mathcal{T}^{(3L)}_{core,\nu\alpha;\lambda\tau}(p_3+p_4,p_3)+(\rho\sigma\leftrightarrow\lambda\tau).\end{aligned}$$

The $F^{(1)}F^{(3)}$ contribution is written as:

$$\Gamma^{abcd,(4)}_{\mu\nu;\rho\sigma\lambda\tau}\Big|_{(1)(3)} = 2\Big[\mathcal{M}^{abcd}_{\mu\nu;\rho\sigma\lambda\tau}(p_i;u_0) - \frac{1}{4}\delta_{\mu\nu}\mathcal{M}^{abcd}_{\alpha\alpha;\rho\sigma\lambda\tau}(p_i;u_0)\Big]. \tag{20}$$

For general kinematics the tensor $\mathcal{M}$ is defined by a permutation sum over the four external gluon legs. However, in the operator tadpole diagram the kinematics specialize to $(p,-p,k,-k)$, and the permutation sum reduces to four non-equivalent assignments corresponding to the four choices of which external leg is absorbed by the linear kernel X. In that case one may write the non-permutation form

$$\begin{aligned}\mathcal{M}^{abcc}_{\mu\nu;\rho\sigma\alpha\beta}(p,-p,k,-k;u_0) =\\ X_{\mu\lambda;\rho}(p;u_0)\mathcal{L}^{bcc}_{\nu\lambda;\sigma\alpha\beta}(-p,-p,k;u_0)\\ +X_{\mu\lambda;\sigma}(-p;u_0)\mathcal{L}^{acc}_{\nu\lambda;\rho\alpha\beta}(p,k,-k;u_0)\\ +X_{\mu\lambda;\alpha}(k;u_0)\mathcal{L}^{abc}_{\nu\lambda;\rho\sigma\beta}(-k,p,-p;u_0)\\ +X_{\mu\lambda;\beta}(-k;u_0)\mathcal{L}^{abc}_{\nu\lambda;\rho\sigma\alpha}(k,p,-p;u_0),\end{aligned}$$

where

$$X_{\mu\lambda;\rho}(q;u_0) = \Omega^{\mu\lambda}_{3L}(q;u_0)\big(\hat{q}_\mu\delta_{\lambda\rho} - \hat{q}_\lambda\delta_{\mu\rho}\big). \tag{21}$$

This representation is particularly convenient in the tadpole channel because it eliminates the explicit sum over S_4 and makes the color contractions transparent. The tadpole-specialized 4-gluon vertex, after color contraction of the two internal legs, becomes

$$\begin{aligned}\Lambda^{abcd,(4)}_{\mu\nu;\rho\sigma\alpha\beta}(p,-p,k,-k;u_0) \;=\; & C_A\delta^{ab}\,[\mathcal{S}_{\mu\lambda;\rho\alpha}(p,k;u_0)\\ & \times\mathcal{S}_{\mu\lambda;\sigma\beta}(-p,-k;u_0)\\ & -\frac{1}{4}\delta_{\mu\nu}\mathcal{S}_{\eta\lambda;\rho\alpha}(p,k;u_0)\\ & \times\mathcal{S}_{\eta\lambda;\sigma\beta}(-p,-k;u_0)]\\ & +2C_A\delta^{ab}\,[\mathcal{M}_{\mu\nu;\rho\sigma\alpha\beta}(p,k;u_0)\\ & -\frac{1}{4}\delta_{\mu\nu}\mathcal{M}_{\lambda\lambda;\rho\sigma\alpha\beta}(p,k;u_0)\Big]\,.\end{aligned} \tag{22}$$

B. One-loop Contributions

The one-loop renormalization is extracted from the one-particle irreducible amputated two-gluon Green function with one EMT insertion,

$$\Gamma^{ab}_{\mu\nu;\rho\sigma}(p) = \langle A^a_\rho(p)\,T_{\mu\nu}(0)\,A^b_\sigma(-p)\rangle\big|_{\text{1PI,amp}}\,. \tag{23}$$

At one loop, the correction separates into three topologies,

$$\Gamma^{(1)} = \Gamma^{(1)}_{\text{sail}} + \Gamma^{(1)}_{\text{tad}} + \Gamma^{(1)}_{\text{leg}}. \tag{24}$$

The contributions to the one-loop correction, from sail (external leg corrections), operator self-energy (tadpole) diagrams, and vertex diagrams, are shown in Fig. 2. The sail diagram is generated by the contraction of the three-gluon EMT vertex with the three-gluon gauge-action vertex through two internal gluon propagators. These represent the one-loop correction to the external gluon wave functions. The virtual gluon loop dresses the incoming or outgoing gluon before it interacts with the EMT operator. These are wave function renormalization corrections to the external gluon legs. These provide part of anomalous dimension (logarithmic divergence) and a lattice-specific finite contribution.

In Landau gauge, the corresponding amputated two-gluon Green function is

$$\begin{aligned}\Gamma^{(1)\,\text{sail},ab}_{\mu\nu;\rho\sigma}(p) \;=\; & \int_{BZ}\frac{d^4k}{(2\pi)^4}\,\Lambda^{ace,(3)}_{\mu\nu;\rho\alpha\beta}(p,-p-k,k;u_0)\\ & \times D^{cc'}_{\alpha\alpha'}(p+k;u_0)\\ & \times V^{bc'e',(3)}_{\sigma\alpha'\beta'}(-p,p+k,-k;u_0)D^{ee'}_{\beta\beta'}(k;u_0),\end{aligned} \tag{25}$$

[1] The Feynman diagrams were generated using the LaTeX package `tikz-feynman`.

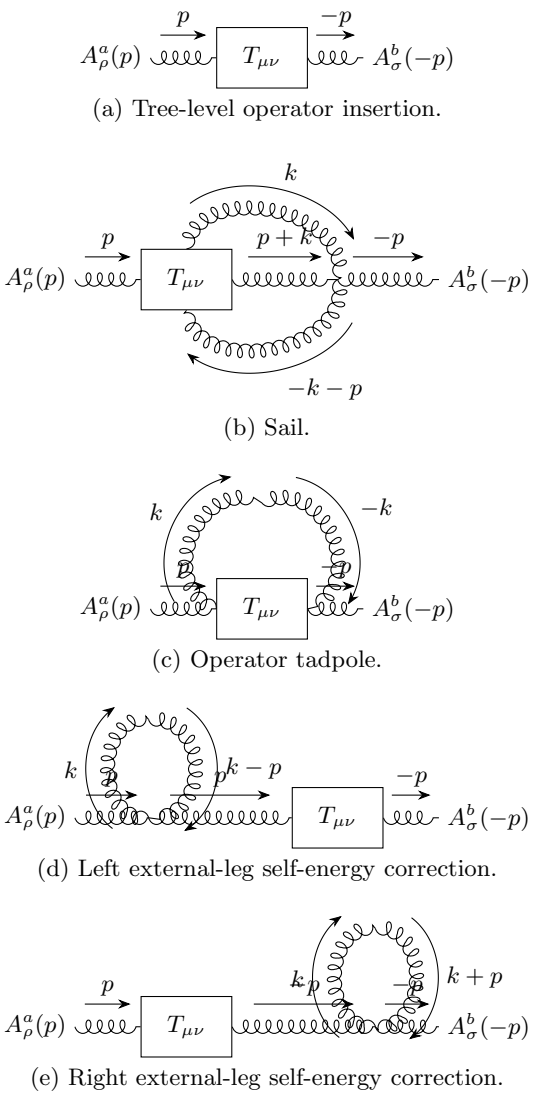

(a) Tree-level operator insertion.

(b) Sail.

(c) Operator tadpole.

(d) Left external-leg self-energy correction.

(e) Right external-leg self-energy correction.

FIG. 2. One-loop Feynman diagrams [b] contributing to the renormalization of the improved gluonic energy–momentum tensor $T_{\mu\nu}$.

where p is the external momentum and k is the loop momentum. The two internal propagators therefore carry momenta $p+k$ and k, respectively. The 3-gluon gauge-action vertex for the tadpole-improved tree-level Symanzik action is

$$\begin{aligned}V^{bc'e',(3)}_{\sigma\alpha'\beta'}(p_1,p_2,p_3;u_0) \;=\; & g_0\,f^{bc'e'}\Big[\frac{c_0}{u_0^4}V^P_{\sigma\alpha'\beta'}(p_1,p_2,p_3)\\ & +\frac{c_1}{u_0^6}V^R_{\sigma\alpha'\beta'}(p_1,p_2,p_3)\Big]\,,\end{aligned} \tag{26}$$

where V^P and V^R denote the plaquette and rectangle parts, respectively. For the sail kinematics used in Eq. (26),

$$(p_1,p_2,p_3) = (-p,p+k,-k). \tag{27}$$

It is convenient to define the transverse projector

$$P_{\alpha\beta}(q) \equiv \delta_{\alpha\beta} - \frac{\hat{q}_\alpha \hat{q}_\beta}{\hat{q}^2}, \tag{28}$$

so that

$$\begin{aligned} D^{cc'}_{\alpha\alpha'}(p+k;u_0) &= \delta^{cc'} \frac{P_{\alpha\alpha'}(p+k)}{\widehat{(p+k)}^2 K_T(p+k;u_0)}, \\ D^{ee'}_{\beta\beta'}(k;u_0) &= \delta^{ee'} \frac{P_{\beta\beta'}(k)}{\hat{k}^2 K_T(k;u_0)}, \end{aligned} \tag{29}$$

with

$$K_T(q;u_0) = \tilde{c}_0 + \tilde{c}_1 a^2 \hat{q}^2,\ \tilde{c}_0 = \frac{5}{3u_0^4} - \frac{2}{3u_0^6},\ \tilde{c}_1 = \frac{1}{12u_0^6},$$

and $\hat{q}_\mu = (2/a)\sin(aq_\mu/2)$.

Substituting Eqs. (17), (26) and (29) in Eq. (25), and noting that the explicit factors of g_0 cancel, one obtains

$$\begin{aligned} \Gamma^{(1,\mathrm{sail},ab)}_{\mu\nu;\rho\sigma}(p) &= 2\int_{BZ} \frac{d^4k}{(2\pi)^4} f^{ace}\delta^{cc'} f^{bc'e'}\delta^{ee'} \\ &\quad \frac{\mathcal{N}^{\mathrm{sail}}_{\mu\nu;\rho\sigma}(p,k;u_0)}{\widehat{(p+k)}^2 K_T(p+k;u_0)\hat{k}^2 K_T(k;u_0)}, \end{aligned}$$

where the numerator is

$$\begin{aligned} \mathcal{N}^{\mathrm{sail}}_{\mu\nu;\rho\sigma}(p,k;u_0) &= [\mathcal{G}_{\mu\nu;\rho\alpha\beta}(p,-p-k,k;u_0) \\ &\quad -\frac{1}{4}\delta_{\mu\nu}\mathcal{G}_{\lambda\lambda;\rho\alpha\beta}(p,-p-k,k;u_0)\Big] \\ &\quad \times P_{\alpha\alpha'}(p+k)\left[\frac{c_0}{u_0^4}V^P_{\sigma\alpha'\beta'}\right. \\ &\quad \left.+\frac{c_1}{u_0^6}V^R_{\sigma\alpha'\beta'}\right] P_{\beta\beta'}(k). \end{aligned} \tag{30}$$

The color contraction is immediate:

$$f^{ace}\delta^{cc'}f^{bc'e'}\delta^{ee'} = f^{ace}f^{bce} = C_A\,\delta^{ab}, \tag{31}$$

and therefore the contribution from the sail diagram reduces to

$$\begin{aligned} \Gamma^{(1)\,\mathrm{sail},ab}_{\mu\nu;\rho\sigma}(p) &= 2C_A\delta^{ab}\int_{BZ}\frac{d^4k}{(2\pi)^4} \\ &\quad \times \frac{\mathcal{N}^{\mathrm{sail}}_{\mu\nu;\rho\sigma}(p,k;u_0)}{\widehat{(p+k)}^2 K_T(p+k;u_0)\,\hat{k}^2 K_T(k;u_0)}. \end{aligned} \tag{32}$$

Using Eq. (18), the numerator may be written explicitly as:

$$\begin{aligned} \mathcal{N}^{\mathrm{sail}}_{\mu\nu;\rho\sigma}(p,k;u_0) &= \Big[X_{\mu\lambda;\rho}(p;u_0)\mathcal{S}^{(3L)}_{\nu\lambda;\alpha\beta}(-p,-p-k;u_0) \\ &\quad +X_{\nu\lambda;\rho}(p;u_0)\mathcal{S}^{(3L)}_{\mu\lambda;\alpha\beta}(-p,-p-k;u_0) \\ &\quad -\frac{1}{2}\delta_{\mu\nu}X_{\eta\lambda;\rho}(p;u_0) \\ &\quad \times\mathcal{S}^{(3L)}_{\eta\lambda;\alpha\beta}(-p,-p-k;u_0)\Big] \\ &\quad \times P_{\alpha\alpha'}(p+k)\left[\frac{c_0}{u_0^4}V^P_{\sigma\alpha'\beta'}(-p,p+k,-k)\right. \\ &\quad \left.+\frac{c_1}{u_0^6}V^R_{\sigma\alpha'\beta'}(-p,p+k,-k)\right] P_{\beta\beta'}(k). \end{aligned} \tag{33}$$

It is useful to separate the core and transport pieces of the clover kernel:

$$\mathcal{K}^{(3L)} = \mathcal{K}^{(3L)}_c + \mathcal{T}^{(3L)}.$$

Accordingly,

$$\mathcal{N}^{\mathrm{sail}} = \mathcal{N}^{\mathrm{sail}}_c + \mathcal{N}^{\mathrm{sail}}_T,$$

with

$$\begin{aligned} \mathcal{N}^{\mathrm{sail}}_c(p,k;u_0) &= \Big[X_{\mu\lambda;\rho}(p)\,\mathcal{S}^{(3L)}_{c,\nu\lambda;\alpha\beta}(-p,-p-k) \\ &\quad +X_{\nu\lambda;\rho}(p)\,\mathcal{S}^{(3L)}_{c,\mu\lambda;\alpha\beta}(-p,-p-k) \\ &\quad -\frac{1}{2}\delta_{\mu\nu}X_{\eta\lambda;\rho}(p)\,\mathcal{S}^{(3L)}_{c,\eta\lambda;\alpha\beta}(-p,-p-k)\Big] \\ &\quad \times P_{\alpha\alpha'}(p+k)\left[\frac{c_0}{u_0^4}V^P_{\sigma\alpha'\beta'}\right. \\ &\quad \left.+\frac{c_1}{u_0^6}V^R_{\sigma\alpha'\beta'}\right] P_{\beta\beta'}(k), \end{aligned} \tag{34}$$

and

$$\begin{aligned} \mathcal{N}^{\mathrm{sail}}_T(p,k;u_0) &= \Big[X_{\mu\lambda;\rho}(p)\mathcal{T}^{(3L)}_{\nu\lambda;\alpha\beta}(-p,-p-k) \\ &\quad +X_{\nu\lambda;\rho}(p)\,\mathcal{T}^{(3L)}_{\mu\lambda;\alpha\beta}(-p,-p-k) \\ &\quad -\frac{1}{2}\delta_{\mu\nu}X_{\eta\lambda;\rho}(p)\,\mathcal{T}^{(3L)}_{\eta\lambda;\alpha\beta}(-p,-p-k)\Big] \\ &\quad \times P_{\alpha\alpha'}(p+k)\left[\frac{c_0}{u_0^4}V^P_{\sigma\alpha'\beta'}\right. \\ &\quad \left.+\frac{c_1}{u_0^6}V^R_{\sigma\alpha'\beta'}\right] P_{\beta\beta'}(k). \end{aligned} \tag{35}$$

The first term $\mathcal{N}^{\mathrm{sail}}_c$ contains the continuum-like vertex structure, while $\mathcal{N}^{\mathrm{sail}}_T$ measures the leading distortion induced by the finite lattice geometry of the clover operator. This split is useful both conceptually and practically, since it separates the continuum matching structure from the genuinely lattice-specific correction.

To obtain the contribution relevant for the renormalization constant, the Green function is projected onto the transverse symmetric-traceless spin-2 channel. We use

$$\begin{aligned} t_{\rho\sigma}(p) &= \delta_{\rho\sigma} - \frac{\hat{p}_\rho \hat{p}_\sigma}{\hat{p}^2}, \\ P_{\mu\nu;\gamma\delta} &= \frac{1}{2}(\delta_{\mu\gamma}\delta_{\nu\delta} + \delta_{\mu\delta}\delta_{\nu\gamma}) - \frac{1}{4}\delta_{\mu\nu}\delta_{\gamma\delta}, \end{aligned}$$

and define

$$\mathcal{F}^{(1)}_{\rm sail}(p;u_0) = P_{\mu\nu;\gamma\delta} t_{\rho\gamma}(p) t_{\sigma\delta}(p) \Gamma^{(1)\rm sail}_{\mu\nu;\rho\sigma}(p;u_0).$$

Substituting Eq. (32) into the above equation gives

$$\begin{aligned} \mathcal{F}^{(1)}_{\rm sail}(p;u_0) &= 2C_A \int_{BZ} \frac{d^4k}{(2\pi)^4} \\ &\quad \times \frac{P_{\mu\nu;\gamma\delta} t_{\rho\gamma}(p) t_{\sigma\delta}(p) \mathcal{N}^{\rm sail}_{\mu\nu;\rho\sigma}(p,k;u_0)}{\widehat{(p+k)}^2 K_T(p+k;u_0)\, \hat{k}^2 K_T(k;u_0)}. \end{aligned} \tag{36}$$

Expanding the projected integrand for small external momentum and retaining the coefficient of the p^2 tensor structure, the sail diagram contributes to the finite one-loop matching coefficient through

$$\mathcal{F}^{(1)}_{\rm sail}(p;u_0) = \frac{g_0^2 C_A}{16\pi^2}\, p^2\, B_{\rm sail}(u_0) + O(p^4), \tag{37}$$

where $B_{\rm sail}(u_0)$ is reduced analytically to the minimal basis of Brillouin-zone integrals

$$\begin{aligned} B_{sail}(u_0) &= \frac{5}{3}\tilde{c}_0^2 I_0(u_0) - \frac{1}{3}\tilde{c}_0^2 I_1(u_0) + \tilde{c}_0^2 \tilde{c}_1 I_2(u_0) \\ &\quad - \frac{7}{6}\tilde{c}_0^2 \sum_{n,m=1}^{3} c_n^{(F)} c_m^{(F)} I^{(0)}_{nm}(u_0) \\ &\quad + \frac{1}{2}\tilde{c}_0^2 \tilde{c}_1 \sum_{n,m=1}^{3} c_n^{(F)} c_m^{(F)} I^{(1)}_{nm}(u_0). \end{aligned} \tag{38}$$

For the isotropic kernel $K_T(k;u_0) = \tilde{c}_0 + \tilde{c}_1 a^2 \hat{k}^2$, the one-loop projected amplitude reduces to the minimal scalar basis

$$\begin{aligned} I_0(u_0) &= \int_{BZ} \frac{d^4k}{(2\pi)^4} \frac{1}{\hat{k}^2 K_T(k;u_0)^2}, \\ I_1(u_0) &= \int_{BZ} \frac{d^4k}{(2\pi)^4} \frac{1}{K_T(k;u_0)^2}, \\ I_2(u_0) &= \int_{BZ} \frac{d^4k}{(2\pi)^4} \frac{1}{\hat{k}^2 K_T(k;u_0)^3}, \end{aligned}$$

together with the operator-weighted integrals

$$\begin{aligned} I^{(0)}_{nm}(u_0) &= \int_{BZ} \frac{d^4k}{(2\pi)^4} \frac{\Phi_{nm}(k)}{\hat{k}^2 K_T(k;u_0)^2}, \\ I^{(1)}_{nm}(u_0) &= \int_{BZ} \frac{d^4k}{(2\pi)^4} \frac{\Phi_{nm}(k)}{\hat{k}^2 K_T(k;u_0)^3}, \end{aligned}$$

where

$$\Phi_{nm}(k) = \frac{1}{4}\sum_{\mu<\nu} \Omega^{\mu\nu}_n(k) \Omega^{\mu\nu}_m(k). \tag{39}$$

In this way the sail contribution is represented by an explicit, gauge-invariant numerator built from the improved EMT kernel, the improved gauge-action vertex, and the transverse lattice propagator, together with a scalar denominator controlled entirely by the improved transverse kernel $K_T(k;u_0)$.

The operator tadpole diagrams arise when the two gluon fields in the operator's $O(A^2)$ vertex contract with each other, forming a closed loop. The operator "feeds on itself" by emitting and reabsorbing virtual gluons. These diagrams are expected to give power divergences that must be subtracted. The contribution from the operator tadpole is given by

$$\begin{aligned} \Gamma^{(1)\,\rm tad,ab}_{\mu\nu;\rho\sigma}(p) &= \frac{1}{2}\int_{BZ} \frac{d^4k}{(2\pi)^4} \Lambda^{abcc,(4)}_{\mu\nu;\rho\sigma\alpha\beta}(p,-p,k,-k;u_0) \\ &\quad \times D^{cc}_{\alpha\beta}(k;u_0). \end{aligned}$$

Using the propagator, the above expression becomes

$$\Gamma^{(1)\,\rm tad,ab}_{\mu\nu;\rho\sigma}(p) = g_0^2 C_A \delta^{ab} \int_{BZ} \frac{d^4k}{(2\pi)^4} \frac{\mathcal{N}^{tad}_{\mu\nu;\rho\sigma}(p,k;u_0)}{\hat{k}^2 K_T(k;u_0)} \tag{40}$$

with

$$\mathcal{N}^{tad}_{\mu\nu;\rho\sigma} = \frac{1}{2}\Lambda^{abcc,(4)}_{\mu\nu;\rho\sigma\alpha\beta}(p,-p,k,-k;u_0)\left(\delta_{\alpha\beta} - \hat{k}_\alpha \hat{k}_\beta/\hat{k}^2\right)$$

The vertex diagrams involve the interaction between the operator and the action vertices. The operator vertex (from expanding $T^{Imp}_{\mu\nu}$ to $O(A^2)$) connects with the action vertex (three-gluon vertex) via gluon propagators. The external-leg contribution generated by the gluon self-energy, is given by

$$\Pi^{ab}_{\rho\sigma}(p) = \delta^{ab}\left[(\delta_{\rho\sigma}\hat{p}^2 - \hat{p}_\rho \hat{p}_\sigma)\Pi_T(p^2;u_0) + \hat{p}_\rho \hat{p}_\sigma \Pi_L(p^2;u_0)\right], \tag{41}$$

and contributes through

$$\Gamma^{(1)\,\rm leg}_{\mu\nu;\rho\sigma}(p) = -2g_0^2\, \Pi_T(\mu^2;u_0)\, \Lambda^{(2)}_{\mu\nu;\rho\sigma}(p;u_0). \tag{42}$$

To extract the renormalization constant, we project onto the transverse symmetric-traceless channel and define

$$\mathcal{F}^{\rm lat}(p;u_0) = P_{\mu\nu;\alpha\beta}\, t_{\rho\alpha}(p) t_{\sigma\beta}(p)\, \Lambda^{\rm lat}_{\mu\nu;\rho\sigma}(p;u_0). \tag{43}$$

The total coefficient is the sum of three one-loop topologies

$$\mathfrak{B}_{\rm lat}(u_0) = \mathfrak{B}^{\rm sail}_{\rm lat}(u_0) + \mathfrak{B}^{\rm tad}_{\rm lat}(u_0) + \mathfrak{B}^{\rm leg}_{\rm lat}(u_0)$$

where

$$\begin{aligned}
\mathfrak{B}^{\rm sail}_{\rm lat}(u_0) &= C^{\rm sail}_0(u_0)I_0(u_0) + C^{\rm sail}_1(u_0)I_1(u_0) \\
&\quad + C^{\rm sail}_2(u_0)I_2(u_0) \\
&\quad + \sum_{n,m=1}^{3}\Big[C^{(0),{\rm sail}}_{nm}(u_0)I^{(0)}_{nm}(u_0) \\
&\quad + C^{(1),{\rm sail}}_{nm}(u_0)I^{(1)}_{nm}(u_0)\Big], \\
\mathfrak{B}^{\rm tad}_{\rm lat}(u_0) &= C^{\rm tad}_0(u_0)I_0(u_0) + \sum_{n,m=1}^{3} C^{(0),{\rm tad}}_{nm}(u_0)I^{(0)}_{nm}(u_0), \\
\mathfrak{B}^{\rm leg}_{\rm lat}(u_0) &= C^{\rm leg}_0(u_0)I_0(u_0) + C^{\rm leg}_1(u_0)I_1(u_0) \\
&\quad + C^{\rm leg}_2(u_0)I_2(u_0),
\end{aligned}$$

with

$$\begin{aligned}
C^{\rm sail}_0(u_0) &= \frac{5}{3}\,\tilde{c}_0(u_0)^2,\; C^{\rm sail}_1(u_0) = -\frac{1}{3}\tilde{c}_0(u_0)^2, \\
C^{\rm sail}_2(u_0) &= \tilde{c}_0(u_0)^2\tilde{c}_1(u_0), \\
C^{(0),{\rm sail}}_{nm}(u_0) &= -\frac{7}{6}c^{(F)}_n c^{(F)}_m \tilde{c}_0(u_0)^2, \\
C^{(1),{\rm sail}}_{nm}(u_0) &= \frac{1}{2}c^{(F)}_n c^{(F)}_m \tilde{c}_0(u_0)^2\tilde{c}_1(u_0), \\
C^{\rm tad}_0(u_0) &= -\frac{1}{4}\tilde{c}_0(u_0)\mathcal{N}_F(u_0), \\
C^{(0),{\rm tad}}_{nm}(u_0) &= \frac{3}{2}c^{(F)}_n c^{(F)}_m \tilde{c}_0(u_0), \\
C^{\rm leg}_0(u_0) &= \frac{13}{3}\mathcal{N}_F(u_0)\tilde{c}_0(u_0)^2, \\
C^{\rm leg}_1(u_0) &= -\frac{2}{3}\mathcal{N}_F(u_0)\tilde{c}_0(u_0)^2, \\
C^{\rm leg}_2(u_0) &= 2\,\mathcal{N}_F(u_0)\tilde{c}_0(u_0)^2\tilde{c}_1(u_0),
\end{aligned}$$

and

$$\mathcal{N}_F(u_0) = 6\left(\frac{3}{2u_0^4} - \frac{3}{5u_0^8} + \frac{1}{10u_0^{12}}\right)^2.$$

The renormalization constant is then given by

$$Z_T(u_0) = 1 + \frac{g_0^2 C_A}{16\pi^2}\left[\mathfrak{B}_{\overline{\rm MS}} - \mathfrak{B}_{\rm lat}(u_0)\right] + O(g_0^4). \quad (44)$$

The renormalized traceless EMT obtained from the one-loop matching is finally defined by

$$T^{R,{\rm TL}}_{\mu\nu} = \left[1 + \frac{g_0^2 C_A}{16\pi^2}\left(\mathfrak{B}_{\overline{\rm MS}} - \mathfrak{B}_{\rm lat}(u_0)\right)\right] T^{\rm TL}_{\mu\nu} + O(g_0^4). \quad (45)$$

C. Yang-Mill Trace Anamoly

The one-loop renormalization derived in the spin-2 channel determines the normalization of the *traceless* part of the improved gluonic energy–momentum tensor (EMT), but it does not by itself account for the anomalous trace. For the tadpole-improved operator,

$$T^{\rm imp}_{\mu\nu}(x) = \frac{1}{g_0^2}\left[F^{3L}_{\mu\alpha}(x)F^{3L}_{\nu\alpha}(x) - \frac{1}{4}\delta_{\mu\nu}\,F^{3L}_{\alpha\beta}(x)F^{3L}_{\alpha\beta}(x)\right], \quad (46)$$

the classical trace vanishes identically in $d = 4$,

$$\delta_{\mu\nu}T^{\rm imp}_{\mu\nu}(x) = 0, \quad (47)$$

so the operator is classically traceless. The quantum trace anomaly therefore cannot originate from the multiplicative spin-2 renormalization constant alone. Instead, it resides in the scalar trace channel and must be incorporated through the full renormalized EMT rather than through its traceless projection only. Accordingly, the renormalized EMT must therefore be written as

$$T^R_{\mu\nu} = Z_T(u_0)\,T^{\rm imp,TL}_{\mu\nu} + \frac{1}{4}\delta_{\mu\nu}\,Z_\Theta(u_0, a\mu)\,\Theta^{\rm imp}(a), \quad (48)$$

with

$$\Theta^{\rm imp}(a) = \frac{1}{g_0^2}\,\mathcal{O}^{\rm imp}_S(a) = \frac{1}{g_0^2}\,F^{3L}_{\rho\sigma}(a)F^{3L}_{\rho\sigma}(a). \quad (49)$$

The anomaly condition requires

$$\Theta^R(\mu) = \frac{\beta(g)}{2g}\,F^a_{\rho\sigma}F^a_{\rho\sigma}, \quad (50)$$

or equivalently

$$Z_\Theta(u_0, a\mu)\,\frac{1}{g_0^2}\,F^{3L}_{\rho\sigma}F^{3L}_{\rho\sigma} = \frac{\beta(g)}{2g}\,F^a_{\rho\sigma}F^a_{\rho\sigma}. \quad (51)$$

Since the improved clover combination reproduces the continuum field strength up to discretization errors,

$$F^{3L}_{\rho\sigma}F^{3L}_{\rho\sigma} = F^a_{\rho\sigma}F^a_{\rho\sigma} + O(a^2), \quad (52)$$

the matching condition becomes

$$\frac{Z_\Theta(u_0, a\mu)}{g_0^2} = \frac{\beta(g)}{2g} + O(g^4, a^2). \quad (53)$$

Thus the u_0-improved construction modifies the finite lattice matching coefficients, but it does not alter the anomaly coefficient itself.

At one loop in pure Yang–Mills theory,

$$\beta(g) = -\beta_0\,\frac{g^3}{16\pi^2} + O(g^5), \qquad \beta_0 = \frac{11}{3}C_A, \quad (54)$$

so that

$$\frac{\beta(g)}{2g} = -\frac{\beta_0}{2}\frac{g^2}{16\pi^2} + O(g^4) = -\frac{11\,C_A}{6}\frac{g^2}{16\pi^2} + O(g^4). \quad (55)$$

Therefore the renormalized trace must be

$$T^\mu_{\ \mu} = -\frac{11\,C_A}{6}\,\frac{g^2}{16\pi^2}\,F^a_{\rho\sigma}F^a_{\rho\sigma} + O(g^4), \quad (56)$$

which is precisely the one-loop Yang–Mills trace anomaly. In the improved lattice formulation this implies

$$T^{\mu}_{\mu,R} = -\frac{11\,C_A}{6}\,\frac{g^2}{16\pi^2}\,F^a_{\rho\sigma}F^a_{\rho\sigma} + O(g^4, a^2). \tag{57}$$

An equivalent lattice interpretation follows from the relation between the EMT trace and the response of the action to a scale variation or anisotropy. Since $T^{\mu}_{\mu} \sim a\,\partial S/\partial a$, while the bare action depends on a through the bare coupling $g_0(a)$, one finds

$$a\frac{\partial S}{\partial a} = \frac{\partial S}{\partial g_0}\,a\frac{dg_0}{da} \propto \beta(g)\,\frac{\partial S}{\partial g}, \tag{58}$$

and, because $\partial S/\partial g \propto g^{-3}F^2$, this again yields

$$T^{\mu}_{\mu} = \frac{\beta(g)}{2g}\,F^2. \tag{59}$$

Hence the anomaly follows directly from the running of the coupling in the gauge action, and the improved EMT must reproduce it because it is built from the same improved field-strength basis that matches the continuum action density.

Combining the traceless and scalar sectors, the correct renormalized EMT is therefore

$$T^R_{\mu\nu} = Z_T(u_0)\,T^{\mathrm{imp,TL}}_{\mu\nu} + \frac{1}{4}\delta_{\mu\nu}\left[\frac{\beta(g)}{2g}\,F^a_{\rho\sigma}F^a_{\rho\sigma}\right] + O(a^2, g^4). \tag{60}$$

Taking the trace gives

$$\delta_{\mu\nu}T^R_{\mu\nu} = \frac{\beta(g)}{2g}\,F^a_{\rho\sigma}F^a_{\rho\sigma} + O(a^2, g^4), \tag{61}$$

because the traceless component satisfies

$$\delta_{\mu\nu}T^{R,\mathrm{TL}}_{\mu\nu} = 0. \tag{62}$$

Thus, the renormalization procedure based on the improved clover EMT correctly reproduces the quantum trace anomaly while preserving the properly normalized spin-2 part of the gluonic energy-momentum tensor.

We define the connected renormalized Euclidean correlator in the 00 channel by

$$\begin{aligned} G^R_{00}(\tau) &\equiv \int d^3x \left\langle \delta T^R_{00}(\tau,\mathbf{x})\,\delta T^R_{00}(0,\mathbf{0})\right\rangle, \\ \delta T^R_{00} &\equiv T^R_{00} - \langle T^R_{00}\rangle. \end{aligned}$$

The corresponding dimensionless normalized correlator is

$$C^R_{00}(\tau) \equiv \frac{1}{T^5}\,G^R_{00}(\tau) = \frac{1}{T^5}\int d^3x \left\langle \delta T^R_{00}(\tau,\mathbf{x})\,\delta T^R_{00}(0,\mathbf{0})\right\rangle. \tag{63}$$

Using

$$\begin{aligned} T^R_{\mu\nu} &= Z_T(u_0)\,T^{\mathrm{imp,TL}}_{\mu\nu} + \frac{1}{4}\,\delta_{\mu\nu}\,\Theta + O(a^2, g^4), \\ \Theta &\equiv \frac{\beta(g)}{2g}F^a_{\rho\sigma}F^a_{\rho\sigma}, \end{aligned} \tag{64}$$

the 00 component becomes

$$T^R_{00} = Z_T(u_0)\,T^{\mathrm{imp,TL}}_{00} + \frac{1}{4}\,\Theta + O(a^2, g^4), \tag{65}$$

and hence

$$\begin{aligned} G^R_{00}(\tau) &= Z_T^2(u_0)\,G^{\mathrm{imp,TL}}_{00}(\tau) + \frac{Z_T(u_0)}{2}\,G^{\mathrm{mix}}_{0\Theta}(\tau) \\ &\quad + \frac{1}{16}\,G_{\Theta\Theta}(\tau) + O(a^2, g^4), \end{aligned} \tag{66}$$

where

$$\begin{aligned} G^{\mathrm{imp,TL}}_{00}(\tau) &\equiv \int d^3x \Big\langle \delta T^{\mathrm{imp,TL}}_{00}(\tau,\mathbf{x})\delta T^{\mathrm{imp,TL}}_{00}(0,\mathbf{0})\Big\rangle \\ G^{\mathrm{mix}}_{0\Theta}(\tau) &\equiv \int d^3x \Big\langle \delta T^{\mathrm{imp,TL}}_{00}(\tau,\mathbf{x})\delta\Theta(0,\mathbf{0}) \\ &\quad + \delta\Theta(\tau,\mathbf{x})\,\delta T^{\mathrm{imp,TL}}_{00}(0,\mathbf{0})\Big\rangle, \\ G_{\Theta\Theta}(\tau) &\equiv \int d^3x \Big\langle \delta\Theta(\tau,\mathbf{x})\,\delta\Theta(0,\mathbf{0})\Big\rangle. \end{aligned}$$

Therefore,

$$\begin{aligned} C^R_{00}(\tau) &= \frac{1}{T^5}\left[Z_T^2(u_0)\,G^{\mathrm{imp,TL}}_{00}(\tau) + \frac{Z_T(u_0)}{2}\,G^{\mathrm{mix}}_{0\Theta}(\tau)\right. \\ &\quad \left. + \frac{1}{16}\,G_{\Theta\Theta}(\tau)\right] + O(a^2, g^4). \end{aligned} \tag{67}$$

In our formulation, the renormalized energy density T^R_{00} receives both a multiplicative factor $Z_T(u_0)$ acting on the improved traceless operator and an additive contribution from the trace-anomaly operator $\Theta = [\beta(g)/2g]F^2$. Consequently, the correlator $C^R_{00}(\tau)$ is not simply a rescaled version of the bare correlator, but contains additional mixed and pure-anomaly contributions. At leading order the renormalization affects both the overall magnitude and the detailed structure of the correlator. Physically, this modifies the short-distance behavior and can introduce deviations from an ideal plateau at intermediate τT due to mixing with the scalar (trace) channel. Proper renormalization is therefore essential to ensure that the extracted plateau value correctly reproduces the thermodynamic observable c_V/T^3.

IV. COMPARISON OF ONE-LOOP PERTURBATION THEORY WITH THE LATTICE DATA

To assess the reliability of the perturbative matching factor $Z_T(u_0)$, it is essential to compare the one-loop prediction with nonperturbative lattice data obtained from the same improved gauge action and operator basis to quantify the size of residual higher-order and discretization effects, thereby indicating the range of lattice spacings for which the one-loop expression remains quantitatively reliable. The inferred continuum finite part

$\mathfrak{B}^{\rm eff}_{\overline{\rm MS}}$ was determined by matching the lattice-side one-loop formula to the published dashed perturbative curve for $Z_T(g_0^2)$ [13];

$$\mathfrak{B}^{\rm eff}_{\overline{\rm MS}} = \mathfrak{B}_{\rm lat}(u_0) + \frac{16\pi^2}{g_0^2 C_A}\big[Z_T^{\rm curve}(g_0^2) - 1\big].$$

Applying this point by point to the available (g_0^2, u_0) values yielded a nearly constant result, from which the effective value $\mathfrak{B}^{\rm eff}_{\overline{\rm MS}} = 15.04$ was extracted and is approximately constant across the relevant coupling range. Thus 15.04 should be understood as the effective continuum finite matching coefficient that reproduces the published perturbative one-loop normalization in the same projector convention, rather than as a universal constant of the theory. Thus the one-loop renormalization factor is computed as

$$Z_T^{\text{1-loop}}(u_0, g_0^2) = 1 + \frac{g_0^2 C_A}{16\pi^2}\big[15.04 - \mathfrak{B}_{\rm lat}(u_0)\big]. \quad (68)$$

By contrast, the pointwise values $\mathfrak{B}^{\rm eff}_{\overline{\rm MS}}(g_0^2)$ extracted from non-perturbative lattice data should not be used as input for a one-loop prediction, since they already absorb higher-order and non-perturbative effects. Table I shows that the dominant contribution to $\mathfrak{B}_{\rm lat}(u_0)$ comes from the external-leg term, while the tadpole contribution is positive but much smaller, and the sail contribution is negative. The corrected one-loop prediction $Z_T^{\text{1-loop}}$ follows the perturbative curve closely but remains systematically below the continuum-extrapolated lattice data, with the discrepancy increasing monotonically from weak to moderate coupling. The discrepancy grows with g_0^2: it is moderate at intermediate coupling, and becomes large near $g_0^2 \simeq 1$, where the lattice value is about 1.6 while the one-loop curve is only about 1.27. This indicates that the one-loop calculation captures the leading trend but misses sizable higher-order and/or nonperturbative contributions, which enhance the growth of Z_T at moderate coupling. This provides quantitative evidence that the one-loop matching captures the correct normalization trend but does not fully account for the stronger growth of Z_T seen in the lattice calculation. This strongly suggests that higher-order perturbative terms, and possibly additional nonperturbative effects, are required for quantitative agreement beyond the weak-coupling regime

To make the comparison with Fig. 3 more quantitative, we fit the continuum-extrapolated lattice data for Z_T as a function of g_0^2 with a simple cubic ansatz,

$$Z_T^{\rm lat}(g_0^2) = a_0 + a_1 g_0^2 + a_2 (g_0^2)^2 + a_3 (g_0^2)^3. \quad (69)$$

and obtain the effective two-loop and cubic fits using the lattice data from Ref. [13] to provide a phenomenological estimate of higher-loop effects beyond the one-loop calculation. These fits reproduce the lattice curve accurately over the interval $0 \le g_0^2 \le 1$, with an rms deviation of order 6×10^{-3}.

In our explicit calculation, however, the perturbative curve is understood as the full matching factor. The lattice finite contribution itself is comparatively small, $\mathfrak{B}_{\rm lat}(u_0) \simeq 0.41$–$0.61$, so the magnitude of the perturbative curve is controlled predominantly by the continuum–lattice difference $\mathfrak{B}^{\rm eff}_{\overline{\rm MS}} - \mathfrak{B}_{\rm lat}(u_0)$. The

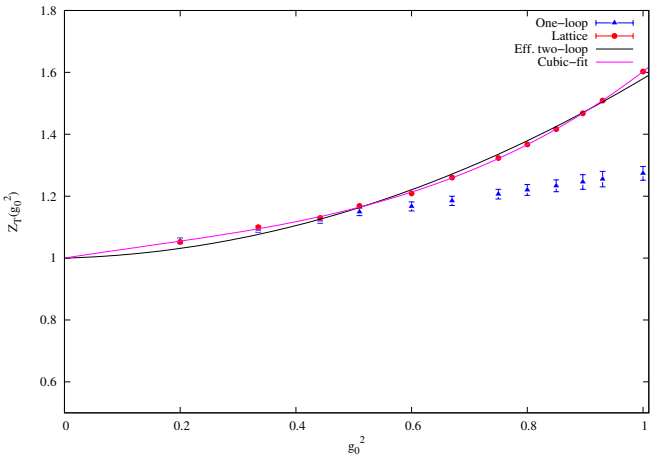

FIG. 3. The renormalization factor $Z_T(g_0^2)$ together with the one-loop analytic result in Eq. (68)

comparison between Eqs. (68) and (69) and makes the origin of the discrepancy transparent. Because the present operator is tadpole improved and built from the three-loop clover combination, one expects the one-loop prediction to show significantly improved agreement with lattice data compared with the unimproved plaquette-clover operator. In particular, the explicit u_0-dependence resums an important subset of mean-field corrections and should reduce the magnitude of finite renormalization effects at moderate lattice couplings.

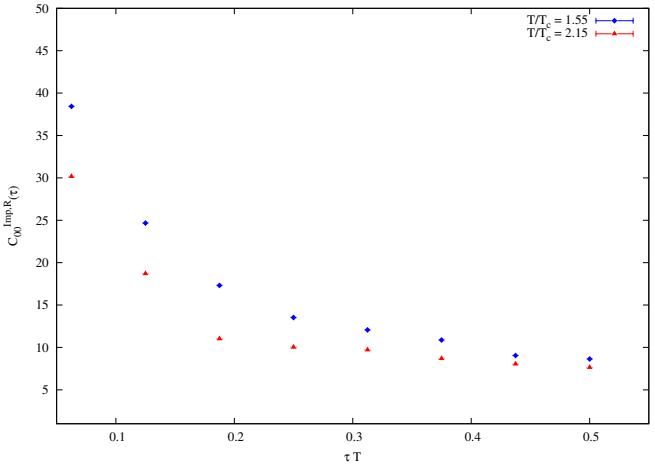

FIG. 4. The anomaly correlator $C_{00}(\tau T)$ on $N_\tau = 16$ lattices.

TABLE I. One-loop lattice contributions and renormalization factor computed with the effective inferred continuum finite term $\mathfrak{B}_{\overline{\rm MS}}^{\rm eff}$.

g_0^2	u_0	$\mathfrak{B}_{\rm sail}$	$\mathfrak{B}_{\rm tad}$	$\mathfrak{B}_{\rm leg}$	$\mathfrak{B}_{\rm lat}$	$Z_T^{\text{1-loop}}$
0.335	0.952	-0.204527	0.131404	0.484903	0.411779	1.093(2)
0.442	0.943	-0.209848	0.133627	0.505208	0.428987	1.123(2)
0.512	0.937	-0.213314	0.135036	0.518870	1 0.440591	1.149(3)
0.605	0.930	-0.217255	0.136592	0.534907	0.454244	1.168(3)
0.750	0.901	-0.231816	0.141737	0.601840	0.511760	1.207(7)
0.850	0.872	-0.241867	0.143884	0.668342	0.570359	1.236(7)
0.930	0.861	-0.243974	0.143618	0.693388	0.593032	1.255(7)
1.000	0.853	-0.244781	0.142970	0.711654	0.609842	1.274(6)

Figure 4 displays the normalized Euclidean energy-density correlator $C_{00}(\tau T)$ for $T/T_c = 1.55$ and 2.15. The correlator exhibits a pronounced decrease with increasing Euclidean time separation, with the strongest signal at small τT and a gradual flattening toward the midpoint $\tau T = 0.5$. Over the full range, the magnitude of the 00-channel fluctuations increases with temperature. The enhancement at small τT is consistent with dominant short-distance ultraviolet contributions, while the weaker variation at larger τT indicates that these ultraviolet effects become less important as the temporal separation increases. Overall, the figure suggests that the temperature dependence primarily enters through the overall normalization of the correlator, whereas the qualitative τT-dependence remains similar for both ensembles.

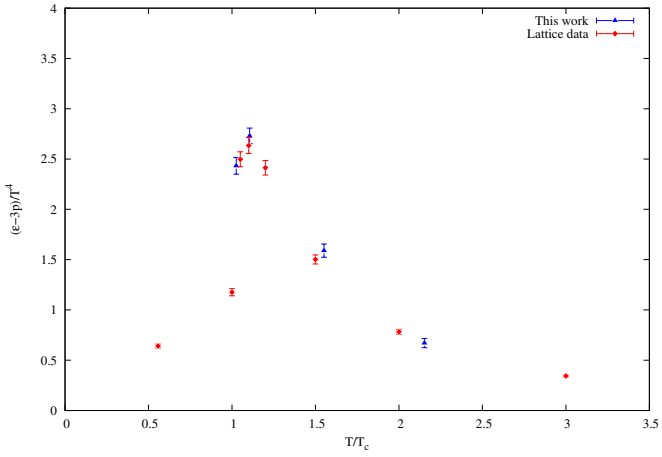

FIG. 5. The trace anomaly for improved EMT. The reference lattice data values are taken from continuum-extrapolated SU(3) lattice equation-of-state results and their Padé interpolation, with the discontinuity at T_c corresponding to the latent heat of the first-order transition [22, 23].

The figure 5 shows the comparison of temperature dependence of the trace anomaly of the present EMT results with reference lattice data [22–24] at $N_\tau = 16$ The trace anomaly rises rapidly from low temperatures as the system approaches the deconfinement region, reaching a pronounced maximum around $T/T_c = 1.0 - 1.2$. This peak reflects the strongest breaking of conformal symmetry and the dominance of nonperturbative dynamics near the transition. At higher temperatures, the trace anomaly decreases steadily, indicating that the system gradually approaches the weakly coupled, approximately conformal regime where $\epsilon \equiv 3p$. The improved EMT results reproduce both the location and magnitude of the peak and show good overall agreement with the lattice data across the full temperature range, with only minor deviations at intermediate temperatures. This behavior is consistent with the expected thermodynamics of the gluon plasma, where nonconformality is maximal near T_c, and diminishes at higher temperatures [22, 25].

V. SUMMARY AND CONCLUSION

In this work, we have presented a complete one-loop renormalization of the gluonic energy–momentum tensor (EMT) in pure SU(3) lattice gauge theory using a tadpole-improved tree-level Symanzik action and a three-loop improved clover discretization of the field-strength tensor. The calculation was carried out in Landau gauge, with matching to the continuum $\overline{\rm MS}$ scheme through a symmetric subtraction procedure. A central achievement of this study is the systematic reduction of all one-loop contributions—sail, tadpole, and external-leg diagrams—into a minimal basis of scalar Brillouin-zone integrals, yielding closed-form expressions for the lattice finite coefficient $\mathfrak{B}_{\rm lat}$ and the renormalization factor $Z_T(u_0)$.

A key structural result is the clean separation between the traceless spin-2 sector and the scalar trace channel. The multiplicative renormalization constant $Z_T(u_0)$, determined through projection onto the transverse symmetric-traceless channel, correctly fixes the normalization of the spin-2 component of the EMT. At the same time, we have demonstrated explicitly that the quantum trace anomaly originates entirely from the scalar operator proportional to $F^a_{\rho\sigma}F^a_{\rho\sigma}$, and is not affected by the spin-2 renormalization. The improved lattice construction reproduces the continuum Yang–Mills trace anomaly at one loop, confirming the consistency of the renormalization procedure and the correctness of the

operator basis.

The use of tadpole improvement and multi-loop clover discretization plays a crucial role in controlling lattice artifacts. By absorbing large renormalizations into powers of the mean-field factor u_0, the perturbative expansion is significantly stabilized, and all one-loop diagrams are rendered ultraviolet finite after tadpole subtraction. Moreover, the decomposition of loop contributions into continuum-like "core" terms and lattice-specific "transport" corrections provides a transparent understanding of how discretization effects enter and how they are systematically suppressed.

We have further shown that renormalization has a nontrivial impact on Euclidean correlators, particularly in the 00-channel. The renormalized correlator is not a simple rescaling of the bare one, but receives additional mixed and scalar-channel contributions arising from the trace anomaly. This modifies both the normalization and the short-distance structure of the correlator, with direct implications for the extraction of thermodynamic quantities such as the specific heat. Consistency between perturbative normalization and nonperturbative lattice data therefore requires a careful implementation of the full renormalized EMT.

Finally, comparison with available lattice results demonstrates that the improved EMT framework reproduces the expected thermodynamic behavior, including the trace anomaly and its temperature dependence, with good agreement. Residual deviations can be attributed to higher-order perturbative corrections and finite lattice spacing effects, suggesting that the present one-loop calculation provides a reliable baseline for quantitative studies.

In conclusion, the tadpole-improved Symanzik EMT constructed and renormalized in this work provides a robust and systematically improvable framework for lattice QCD thermodynamics. It ensures correct normalization of both the spin-2 and scalar sectors, reproduces the continuum trace anomaly, and is well suited for applications to the equation of state, gluon condensates, and transport properties. Future extensions to two-loop order and to full QCD with dynamical fermions, as well as integration with nonperturbative renormalization schemes such as gradient flow, will further enhance the precision and applicability of this approach.

VI. ACKNOWLEDGEMENTS

ML thankfully acknowledges the computer resources provided by the National Supercomputing Center, Zhengzhou.

[1] A. Freese, *Noether's theorems and the energy-momentum tensor in quantum gauge theories.*, Phys. Rev. D, **106**(12), 125012 (2020).

[2] A. Freese, *Reflections on Noether's second theorem and the energy-momentum tensor*, Phys. Rev. D, **113**(1), 016011 (2026)

[3] Y, Yang, *et al.*, *Nonperturbatively renormalized glue momentum fraction at the physical pion mass from lattice QCD*. Phys. Rev. D, **98**(7), 074506 (2018)

[4] C. Alexandrou *et al.*, *Complete flavor decomposition of the spin and momentum fraction of the proton using lattice QCD simulations at physical pion mass*. Phy. Rev. D, **101**(9), 094513 (2020)

[5] Z, Haghani and T. Harko, *The first variation of the matter energy-momentum tensor with respect to the metric, and its implications on modified gravity theories*. Physics of the Dark Universe, **44**, 101462 (2024)

[6] M. Asakawa *et al.*, *Thermodynamics of SU(3) gauge theory from gradient flow on the lattice*. Phys. Rev. D, **90**(1), 011501(R) (2014)

[7] X. Cao, *et al.*, *Energy momentum tensor on and off the light cone: exposition with scalar Yukawa theory*. JHEP, **2024**(7), 95 (2024)

[8] X. Cao, *et al.*, *Energy momentum tensor on and off the light cone: exposition with scalar Yukawa theory*. JHEP, **2024**(7), 95 (2024)

[9] M. Lüscher and P. Weisz, *On-shell improved lattice gauge theories*, Commun. Math. Phys. **97**, 59 (1985); Erratum: Commun. Math. Phys. **98**, 433 (1985).

[10] S. Caracciolo, G. Curci, P. Menotti and A. Pelissetto, *The energy-momentum tensor for lattice gauge theories*, Ann. Phys. **197**, 119 (1990).

[11] S. Capitani and G. Rossi, *Deep inelastic scattering in improved lattice QCD (I). The first moment of structure functions*, Nucl. Phys. B **433**, 351 (1995)],

[12] L. Giusti and H. Meyer, *Thermal Momentum Distribution from Path Integrals with Shifted Boundary Conditions*, Phys. Rev. Lett. **106**, 131601 (2011).

[13] L. Giusti and M. Pepe, *Energy-momentum tensor on the lattice: Nonperturbative renormalization in Yang-Mills theory*, Phys. Rev. D **91**, 114504 (2015)

[14] M. Brida, L. Giusti, and M. Pepe, *Non-perturbative definition of the QCD energy-momentum tensor on the lattice*, JHEP, **04**, 043 (2020)

[15] H. Suzuki, *Energy–momentum tensor from the Yang–Mills gradient flow*, Prog. Theor. Exp. Phys. **2013**, 083B03 (2013).

[16] H. Makino and H. Suzuki, *Lattice energy–momentum tensor from the Yang–Mills gradient flow—inclusion of fermion fields*, Prog. Theor. Exp. Phys. **2014**, 063B02 (2014).

[17] G. P. Lepage and P. B. Mackenzie, *Viability of lattice perturbation theory*, Phys. Rev. D **48**, 2250 (1993).

[18] S. Caracciolo, P. Menotti and A. Pelissetto, *One-loop analytic computation of the energy-momentum tensor for lattice gauge theories*, Nucl. Phys. B **375**, 195 (1992).

[19] S. Capitani, *Lattice perturbation theory*, Phys. Rept. **382**, 113 (2003).

[20] M Costa *et al.*, *Gauge-invariant renormalization scheme in QCD: Application to fermion bilinears and the energy-momentum tensor*, Phys. Rev. D **103**, 094509 (2021).

[21] G. Lepage and P. Mackenzie, *On the viability of lattice perturbation theory*, Phys. Rev D **48**, 2250 (1993).
[22] S. Borsányi *et al.*, *High-precision scale setting in lattice QCD*, JHEP **09**, 10 (2012).
[23] S. Borsányi *et al.*, *Full result for the QCD equation of state with 2+1 flavors*, Phys. Lett. B **730**, 99 (2014).
[24] H. Meyer, *Transport properties of the quark–gluon plasma: A lattice QCD perspective*, Eur. Phys. J. A **47**, 86 (2011).
[25] L. Giusti and M. Pepe, *Equation of state of the SU(3) Yang-Mills theory: a precise determination from a moving frame*, Phys. Letts. B **769**, 385 (2017).